# Multibeam Lasing Action from Bound States in the Continuum of Photonic Crystal Slab Waveguides

**J. T. Wang, D. Lei, M. Tang, and N. C. Panoiu**

University College London, Department of Electronic and Electrical Engineering, Torrington Place, WC1E 7JE, London, United Kingdom

**Abstract**— The ability to create optical resonances with high quality-($Q$) factors makes photonic crystals (PhCs) an ideal platform for enhanced light-matter interaction, and facilitates the design of efficient active photonic devices at the nanoscale. Here, we utilize the physics of optical bound states in the continuum (BICs) to achieve high-$Q$ resonances in two-dimensional PhC slab waveguides and propose a theoretical design for multibeam lasing action. The proposed PhC slab working at 1300 nm supports a quasi-BIC at a wavelength above the diffraction limit. Utilizing Fourier analysis, the optical far-field emitted by the quasi-BIC is investigated and the results show that the zeroth and first diffraction orders are characterized by a topological charge equal to 1. Due to this topological nature of the quasi-BIC, multiple vortex beams are generated into all available diffraction channels. We believe that our multibeam, quantum-dot laser device based on PhC slab waveguides possessing BICs paves a novel way to generate and control laser emission, thus advancing both fundamental research and practical applications in photonics.

## 1. INTRODUCTION

Optical bound states in the continuum (BICs) lie inside the radiation spectrum spanned by propagating waves of free space, but do not emit any optical power into the far-field [1, 2, 3]. A plethora of fundamental research and practical applications utilizing BICs have been reported in nanophotonics within the past decade, ranging from lasing [4, 5, 6] to nonlinear optics [7, 8, 9]. Generally speaking, there are two types of BICs in periodic nanostructures: symmetry-protected BICs arising from the symmetry mismatch between the eigenmodes of an optical system and the radiative channels, and accidental BICs formed *via* structural parameter tuning. Both types of BICs are completely decoupled from all radiation channels, leading to an infinite quality($Q$)-factor and lifetime. Using the physics of BICs, high-$Q$ optical resonances that facilitate strong light-matter interaction can be readily designed applied to manipulate optical response in photonic platforms, including photonic crystals (PhC) [5, 6, 10] and metasurfaces [7, 11].

The topological nature of optical BICs was first studied a decade ago [2], where it was demonstrated that BICs are vortex centers of far-field polarization vectors. On this basis, BICs can be understood and explored with the help of topological charges defined by the winding properties of polarization vector in the **k**-space. Recently, it has been reported [5, 6] the generation of vortex beams and lasers using polarization vortices centered at BICs in the **k**-space, thus allowing a plethora of exciting developments in topological photonics and quantum communications.

A commonly used idea is that BICs of periodic structures exist in the spectral region below the diffraction limit and above the light line, in which case only the zero-order Fourier coefficient needs to be considered [12, 13]. For resonances above the diffraction limit, there exist no true BICs because of the presence of additional energy leakage into higher-order diffraction channels. Accordingly, to date, there has hardly been any interest in BICs situated above the diffraction limit. However, should one focus on the frequency region above the diffraction limit of periodically patterned nanostructures, it should be feasible to achieve high-$Q$ resonances (quasi-BICs) through mechanisms based on symmetry considerations similar to those that lead to the formation of usual BICs. Furthermore, the topological properties of high-order diffraction channels of such high-$Q$ resonances are worthy of special attention because the winding features of the far-field polarization vectors of diffraction channels imply versatile control of optical beam diffraction. Consequently, such resonances with both high $Q$-factor and nontrivial topological properties of diffraction channels may open up new windows of opportunity for fundamental photonics research, as well as advanced applications in optical field manipulation and quantum communication systems.

In this work, we propose a design of a multibeam lasing device based on a quantum dots (QDs) photonic crystal (PhC) slab waveguide supporting quasi-BICs. The properties of the PhC slab are

studied *via* eigenmode expansion method. The results of this investigation show that there exists a high-$Q$ ($10^5$) TE-like mode with wavelength of 1300 nm, located within the wavelength range spanned by the measured gain spectrum of a QDs wafer. Moreover, we used Fourier analysis to understand the diffraction characteristics of the quasi-BIC mode and demonstrate that all mode diffraction orders possess nontrivial topological charge. This novel photonic device can be viewed as a multibeam topological laser.

## 2. MULTIBEAM LASER: GEOMETRY AND QUANTUM DOT WAFER PARAMETERS

In this section, we describe the geometrical configuration of the proposed QDs-based multibeam laser nanodevice and the corresponding parameters of the QDs wafer used in the design process.

As schematically illustrated in Figure 1(a), a PhC slab waveguide with $C_4$ rotational symmetry is chosen as the platform to generate multiple lasing beams, supporting a total of five diffraction channels, including one zeroth-order and four first-order channels. To determine the geometry parameters of the PhC slab, one needs a complete description of the optical properties of the QDs wafer to be used as the platform for the lasing device [14]. Consequently, we present in Figure 1(b) the measured gain spectrum and in Figure 1(c) the layered composition structure of the QDs wafer. As can be observed, the full width at half maximum of the gain spectrum is about 46 nm (it ranges from 1259 nm to 1305 nm), whereas the center wavelength is equal to 1286 nm. Since the lasing device is designed to be used for optical communication purposes pertaining to data centers, to account for the wavelength-dependent absorption effects, the working wavelength of our laser is chosen to be 1300 nm. At this wavelength the gain from QDs is still relatively large and the attenuation during the propagation of waves is small. In the right panel of Figure 1(c), we show the atomic force microscopy image of the InGaAs QDs layer. Moreover, it should be noted that the QDs wafer to be employed in our design favors the excitation of TE-like modes, so that we restrict our discussion below to the results pertaining to this polarization.

Next, we present the structural details of the PhC slab, inferred from the experimental prerequi-

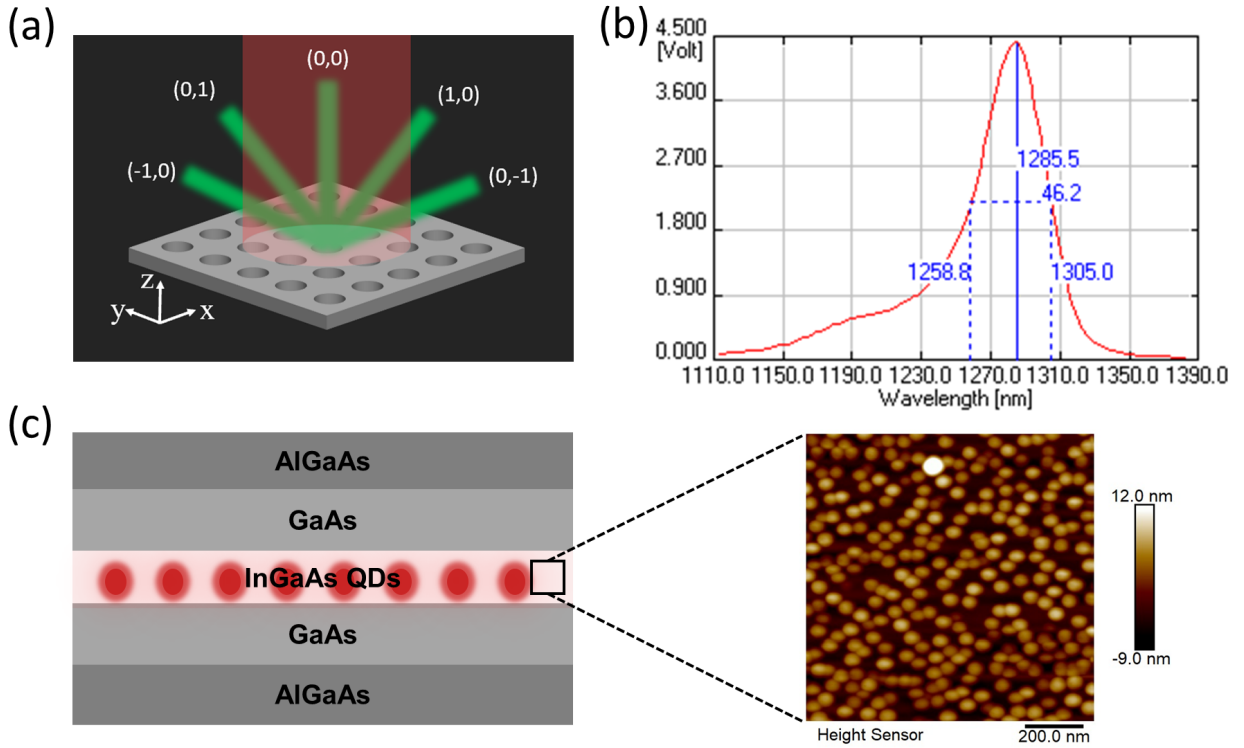


Figure 1: (a) Schematic of a QDs multibeam laser showing a BIC-based PhC slab under the illumination of pump beam (red). The labeled green beams represent the light lasing into different diffraction channels. (b) Measured gain spectrum of QDs wafer. (c) Layered structure and composition of the QDs wafer with a zoom-in showing the atomic force microscopy image of the QDs layer. The red solid circles in the left panel indicate the layer composition of QDs.

sites and desired working wavelength. To simplify the numerical calculations, we set the refractive index of the slab to be 3.4 across the layered structure. This is a reasonable approximation as the index of refraction varies by less than 5% across the layers. The period $a$, thickness of the slab $d$, and radius of the air holes $r$ of the PhC slab were designed to be 1550 nm, 346 nm, and 325 nm, respectively. In addition, we also took into account the tapered nature of the walls of the air holes, induced during the etching fabrication process. Because of this, the up-down symmetry of the PhC slab is broken and therefore there are no true TE or TM modes. In other words, all three components of the electric/magnetic field oriented along $x$-, $y$-, and $z$-axis are different from zero. However, depending on which transverse field component dominates, they can still be viewed as mainly TE/TM polarized.

Considering the designed structure, the first Bragg-diffraction limit wavelength is $\lambda_B = na = 1550$ nm, where $n$ is the index of refraction of the surrounding optical medium (air in our configuration, so that $n = 1$). For the working wavelength of 1300 nm, emission from one zeroth-order and four first-order diffraction channels is permitted to propagate into the far-field.

## 3. EIGENMODE ANALYSIS OF THE DESIGNED NANOSTRUCTURE

In this section, we provide detailed full-wave simulation results that help one understand the optical properties of the modes of the proposed structure. The simulation was performed *via* the finite element method implemented in the Eigenmode solver of COMSOL Multiphysics [15]. Due to the fact that the gain spectrum of the QDs wafer ranges from about 1150 nm to 1350 nm, as per Figure 1(b), we only study the optical modes located within this wavelength range. Additionally, we only consider TE-like eigenmodes, for which the dominant component of the electric field lies within the plane of the PhC slab as this field configuration is the most effective when the field-QDs interaction is considered.

To characterize the intensity of light-matter interaction, we computed the $Q$-factor of the modes by determining their complex-valued frequency. Figure 2(a) presents the spectral location of the TE-like eigenmodes and their corresponding $Q$-factor, all being computed at the Γ-point. Clearly, a mode with particularly large $Q$-factor (nearly $10^5$) can be observed at 1300 nm, and its near-field distribution in the $x$–$y$ cross-section is shown in the inset. Moreover, high-$Q$ modes also exist in the vicinity of 1150 nm, but the relatively low optical gain at this frequency makes it less difficult

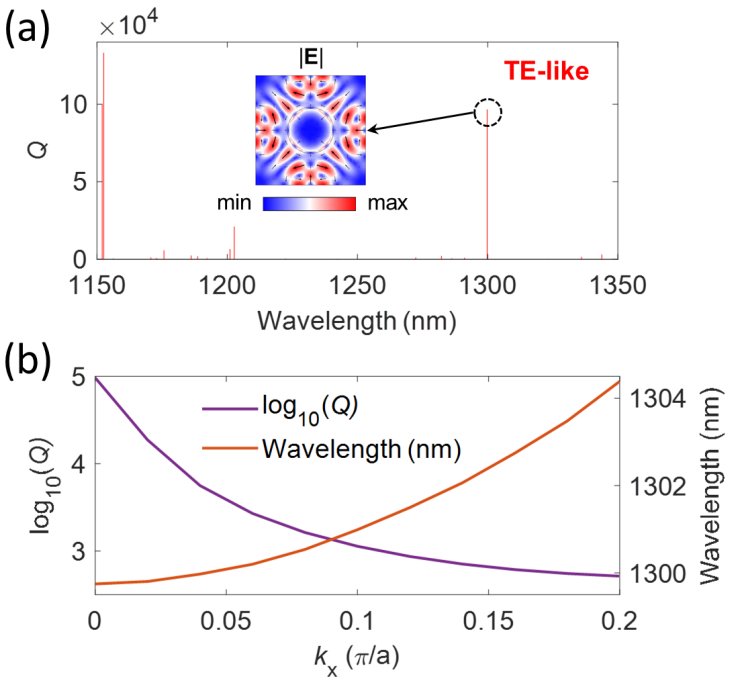


Figure 2: (a) Bar plot of $Q$-factor with respect to the wavelength of TE-like eigenmodes supported by the designed PhC slab, determined at the Γ-point. The inset shows the near-field distribution in the $x$–$y$ cross-section computed for the eigenmode at 1300 nm. (b) Dependence of the resonance wavelength and $Q$-factor of the mode at 1300 nm in (a) on $k_x$, the wavevector component oriented along the ΓX symmetry axis.

to lase as compared to the one at 1300 nm. It is worthy to note that there are quite a few modes in the wavelength domain we considered here. However, owing to either small $Q$-factor, these modes are expected to play no role in the lasing dynamics, so that we will not discuss them any further.

As a further step of our analysis, we now devote special attention to the mode of interest located at 1300 nm, at the Γ-point, and calculate its wavelength dispersion along the ΓX symmetry axis. The results of these calculations are summarized in Figure 2(b). It can be seen that as $k_x$ increases from 0 to $0.2\pi/a$, the resonance wavelength of the mode is slightly red-shifted, increasing from 1300 nm to 1304 nm. By contrast, the $Q$-factor is equal to about $10^5$ at the Γ-point and drops steeply when $k_x$ increases away from the Γ-point. For example, at $k_x = 0.2\pi/a$, the $Q$-factor of the mode is more than two orders of magnitude smaller than its Γ-point value.

## 4. TOPOLOGICAL PROPERTIES OF QUASI-BICS

As described in the last two sections, an eigenmode with wavelength of 1300 nm is found to dominate the gain spectrum of the measured QDs wafer (from 1150 nm to 1350 nm), with its $Q$-factor approaching a magnitude of $10^5$ at the Γ-point. To understand the underlying physics responsible for such a large value of the $Q$-factor, we employed Fourier analysis to study the leakage of energy into the free space and quantify the far-field energy contained in different diffraction orders. The corresponding computational results are illustrated in Figure 3.

Interestingly enough, four diffraction channels containing equal amounts of energy, namely diffraction orders (1,0), (-1,0), (0,1), and (0,-1), play a dominant role in the far-field emission. Compared to the calculated wavelength corresponding to the diffraction limit (1550 nm) for our periodic structure, a good agreement regarding the orders of diffraction is achieved. However, one would expect to observe in the far-field diffraction pattern the (0,0) order, too, but as Figure 3(a) suggests this diffraction order is completely suppressed. This important feature can be understood by considering the in-plane inversion symmetry of the PhC system. More specifically, the complete decoupling of the (0,0) diffraction order from the radiation modes of the free space can be traced to their opposite symmetry. This leads to the large value of the $Q$-factor of this mode, as the amount of energy emitted into the other four diffraction orders is relatively small. From this point of view, we can view this mode as a quasi-BIC situated above the diffraction limit.

Moreover, the topological properties of optical BICs are effective tools to be employed in topological photonics, vortex generation, and quantum communication. The vortex nature of BICs in the $\mathbf{k}$-space can be quantitatively characterized by defining a so-called topological charge, $q$ [2, 16],

$$q = \frac{1}{2\pi} \oint_C d\mathbf{k} \cdot \nabla_{\mathbf{k}} \phi(\mathbf{k}). \tag{1}$$

Here, $C$ represents a closed path in the $\mathbf{k}$-space, which encircles a BIC in the counterclockwise sense, and $\phi(\mathbf{k}) = \arg[c_x(\mathbf{k}) + ic_y(\mathbf{k})]$ is the polarization angle defined by the two-dimensional far-field polarization vector $\mathbf{c}(\mathbf{k})$. In our calculations, the closed path in the $\mathbf{k}$-space was chosen to be a circle centered at the Γ-point and with a radius of $0.5\pi/a$. Under these conditions, the rotation angle of the conserved wavevector $\mathbf{k}$ in the momentum space along this circle can be expressed as $\arg(k_x + ik_y)$.

Using the definition of the topological charge expressed by Equation (1), we first determined the value of $q$ for the zeroth diffraction order. The evolution of polarization angle with respect to the wavevector $\mathbf{k}$ moving along the circle in the $\mathbf{k}$-space is shown in Figure-3(b). A total of $2\pi$ of the accumulation of the polarization angle can be observed in this figure, namely $q = 1$. As we discussed, the frequency of the optical mode is above the diffraction limit, so that four more first-order diffraction channels are allowed. Consequently, we calculated the topological charges of these diffraction orders, too, by considering the corresponding Fourier coefficients. The results of these calculations are given in Figures 3(c) through 3(f). It is evident that all four diffraction channels are characterized by a topological charge equal to 1. In addition, we calculated the emission angle with respect to the normal onto the PhC slab for these four diffraction orders, and found that its value was 56°.

Previous investigations have shown that BIC-based PhC slab waveguides can be effectively employed to generate and manipulation vortex beams. However, previous studies only addressed BICs located below the diffraction limit, case in which only a single beam is generated. Based on our topological analysis presented above, the designed square-lattice PhC slab can produce vortex beams directed along all the existing diffraction channels. The underlying mechanism can be explained by the vortex features of the observed quasi-BIC in the momentum space. These intriguing

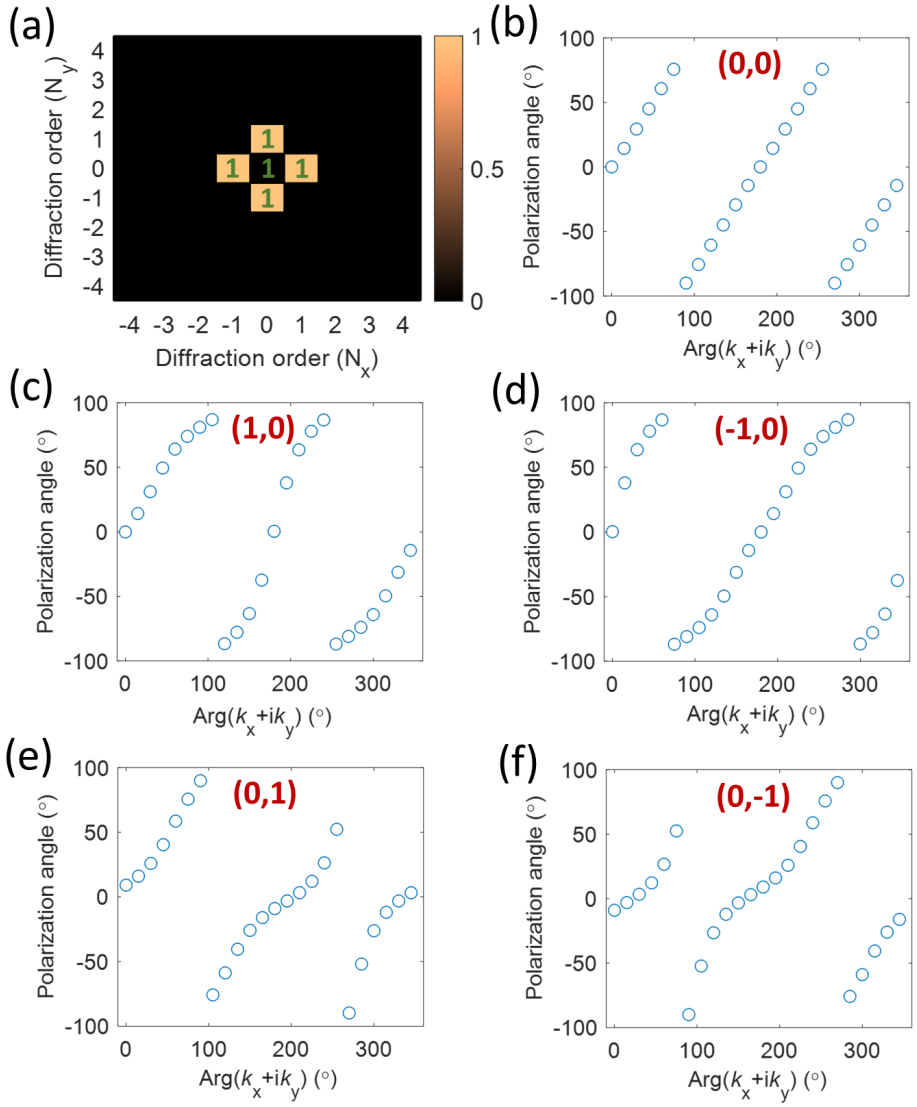


Figure 3: (a) Fourier analysis of the electric far-field within a unit cell of the quasi-BIC mode at the Γ-point. The numbers in different blocks correspond to the topological charge $q$ of each diffraction channel. (b) through (f) Evolution of the polarization angle of polarization ellipse for different diffraction orders along a closed circle path in the **k**-space. In each figure, the order of diffraction is given.

features recommend these quasi-BICs as a prominent platform for the fundamental research and applications of vortex beams.

## 5. CONCLUSION

In conclusion, we presented a novel design of a multibeam laser based on quantum dots PhC slab waveguides. The proposed design supports a quasi-BIC with resonance wavelength of 1300 nm and allows far-field radiation into five diffraction channels. The outgoing flux into the zeroth diffraction order is suppressed by the symmetry incompatibility between the quasi-BIC and radiative modes, whereas the four first-order diffraction channels can transport optical power into the far-field. Importantly, all existing diffraction orders are characterized by a topological charge of 1. Owing to the topology of the quasi-BIC, it is of great interest to study the generation of multiple vortex beams from both a theoretical and experimental perspective. Therefore, the BIC-inspired lasing structure introduced in this work provides a novel route towards topological photonics and quantum communication. As a final point, although we have yet to demonstrate experimentally multibeam lasing into the quasi-BIC investigated in this work, we have successfully observed lasing into a single beam BIC a with a similar $Q$-factor implemented in the same photonic platform.

**REFERENCES**


1. Marinica, D. C., A.G. Borisov and S. V. Shabanov, "Bound states in the continuum in photonics," *Phys. Rev. Lett.*, Vol. 100, No. 18, 183902, 2008.
2. Zhen, B., C. W. Hsu, L. Lu., A. D. Stone and M. Soljacic, "Topological nature of optical bound states in the continuum," *Phys. Rev. Lett.*, Vol. 113, No. 25, 257401, 2014.
3. Hsu, C. W., B. Zhen, A. D. Stone, J. D. Joannopoulos and M. Soljacic, "Bound states in the continuum," *Nat. Rev. Mater.*, Vol. 1, 16048, 2016.
4. Kodigala, A., T. Lepetit, Q. Gu, B. Bahari, Y. Fainman and B. Kante, "Lasing action from photonic bound states in continuum," *Nature*, Vol. 541, No. 7636, 196-199, 2017.
5. Huang, C., C. Zhang, S. Xiao, Y. Wang, Y. Fan, Y. Liu, N. Zhang, G. Qu, H. Ji, J. Han, L. Ge, Y. Kivshar and Q. Song, "Ultrafast control of vortex microlasers," *Science*, Vol. 367, No. 6481, 1018-1021, 2020.
6. Wang, B., W. Liu, M. Zhao, J. Wang, Y. Zhang, A. Chen, F. Guan, X. Liu, L. Shi and J. Zi, "Generating optical vortex beams by momentum-space polarization vortices centered at bound states in the continuum," *Nat. Photonics*, Vol. 14, No. 10, 623-628, 2020.
7. Koshelev, K., Y. Tang, K. Li, D.-Y. Choi, G. Li and Y. Kivshar, "Nonlinear metasurfaces governed by bound states in the continuum," *ACS Photonics*, Vol. 6, No. 7, 1639-1644, 2019.
8. Carletti, L., S. S. Kruk, A. A. Bogdanov, C. De Angelis and Y. Kivshar, "High-harmonic generation at the nanoscale boosted by bound states in the continuum," *Phys. Rev. Res.* , Vol. 1, No. 2, 023016, 2019.
9. Han, Z., F. Ding, Y. Cai and U. Levy, "significantly enhanced second-harmonic generations with all-dielectric antenna array working in the quasi-bound states in the continuum and excited by linearly polarized plane waves," *Nanophotonics*, Vol. 10, No. 3, 1189-1196, 2021.
10. Minkov, M., D. Gerace and S. Fan, "Doubly resonant $\chi^{(2)}$ nonlinear photonic crystal cavity based on a bound state in the continuum," *Optica*, Vol. 121, 263901, 2019.
11. Azzam, S. I. and A. V. Kildishev, "Photonic bound states in the continuum: From basics to applications," *Adv. Opt. Mater.*, Vol. 9, 2001469, 2020.
12. Koshelev, K., G. Favraud, A. Bogdanov, Y. Kivshar and A. Fratalocchi, "Nonradiating photonics with resonant dielectric nanostructures," *Nanophotonics*, Vol. 8, No. 5, 725-745, 2019.
13. Cerjan, A., C. Jörg, S. Vaidya, S. Augustine, W. A. Benalcazar, C. W. Hsu, G. von Freymann and M. C. Rechtsman, "Observation of bound states in the continuum embedded in symmetry bandgaps," *Sci. Adv.*, Vol. 7, No. 52, eabk1117, 2021.
14. Li, H., M. Tang, T. Zhou, W. Xie, R. Li, Y. Gong, M. Martin, T. Baron, S. Chen, H. Liu and Z. Zhang, "Monolithically integrated photonic crystal surface emitters on silicon with a vortex beam by using bound states in the continuum," *Opt. Lett.*, Vol. 48, No. 7, 1702-1705, 2023.
15. COMSOL Multiphysics. Available from: https://www.comsol.com.
16. Yoda, T. and M. Notomi, "Generation and annihilation of topologically protected bound states in the continuum and circularly polarized states by symmetry breaking," *Phys. Rev. Lett.*, Vol. 125, No. 5, 053902, 2020.